Long-term Performance of Engineered Barrier Systems

PEBS

DELIVERABLE (D3.3-2)

Report on the modeling with initially available data

Ola Kristensson, Clay Technology AB

August 2011

SKB

CLAY TECHNOLOGY AB

Table of Contents

Introduction

In the Swedish application for a high level waste repository, a safety assessment report was included. To back up the safety assessment report, a data report, Åkesson et al. (2010a), and a modeling report, Åkesson et al. (2010b), covering some critical scenarios were produced. Among the 22 modeling tasks reported in Åkesson et al. (2010b), 11 included the bentonite buffer, namely:

- Task 1, Peak temperature calculations
- Task 3, Analysis of time scale of buffer hydration
- Task 4, Analysis of moisture redistribution in dry rock scenario
- Task 5, Buffer homogenization
- Task 6, Homogenization after loss of bentonite mass
- Task 8, Buffer upward swelling
- Task 9, Canister sinking
- Task 10, Rock shear trough a deposition hole
- Task 11, Piping and erosion
- Task 18, Bottom plate 1 – Lifting of package
- Task 19, Bottom plate 2 – Buffer swelling after concrete disintegration

Below in the following sections, a brief overview of the 11 tasks including the buffer is given. For the tasks, information is given about: the objective, models used, some main results, and uncertainties. Some of the tasks are thought to be of higher relevance with consideration to the PEBS framework (tasks 3, 4, and 5) and are therefore described in more detail, whereas other, considered being periphery to the PEBS framework, are just briefly described. Issues related to the buffer material models and parameters are discussed in connection with the task (out of 3,4, and 5) that is considered most relevant.

Also, tasks 1 and 10 were not reported in detail in Åkesson et al. (2010b) and therefore an overview is only given here.

For identification, the same task number and title as utilized in Åkesson et al. (2010b) are used. The type of process/processes (Thermal Hydraulic Mechanical) considered are also indicated.

Task 1, Peak temperature calculations (T)

In this task the peak temperature in the buffer was estimated. The actual calculation of the peak temperature was performed in a separate project which aimed at developing a strategy for thermal dimensioning of the final repository for spent nuclear fuel, reported in Hökmark et al. (2009). A brief description was however included in the report reviewed here due to the coupling to task 4, "Analysis of moisture-redistribution in dry rock", which gave input, in form of thermal conductivities, to the peak temperature calculations.

Task 3, Analysis of time scale of buffer hydration (TH)

The time-scale to fully water saturate the buffer was here analyzed. A number of thermo-hydraulic axis-symmetric 2D finite element models (solved with CODE_BRIGHT) were used for the studies. Responses from models with different hydraulic properties and with/without water bearing features were studied and compared.

Important material models for the buffer in this task are advective flow of water,

$$\mathbf{q}_l = -\frac{k k_{rl}}{\mu_l}\nabla p_l$$

$$k_{rl} = S_l^{\lambda}$$

$$\mu_l = 2\cdot 10^{-12}\exp\left(\frac{1808.5}{273.15+T}\right)$$

, with parameters {k, λ, μ_l}, and the water retention model. Two variations of Van Genuchten's retention model have been used. The first, "ordinary",

$$S_l(p_l, p_g) = \left(1+\left(\frac{p_g - p_l}{p}\right)^{\frac{1}{1-\lambda}}\right)^{-\lambda}$$

, with parameters {λ, p} and the second, "new" one (usually called extended Van Genuchten),

$$S_l(p_l, p_g, T) = \left(1+\left(\frac{p_g - p_l}{p(T)}\right)^{\frac{1}{1-\lambda}}\right)^{-\lambda}\left(1-\frac{p_g - p_l}{p_1}\right)^{\lambda_1}$$

$$p(T) = p_0\frac{\sigma(T)}{\sigma_0}$$

$$\sigma(T) = \left(1-0.625\frac{374.15-T}{647.3}\right)\left(0.2358\left(\frac{374.15-T}{647.3}\right)^{1.256}\right)$$

, with parameters {λ, λ_1, p_0, p_1 σ_0}. The graphs of the retention curves used are shown in Figure 1, where also experimental data used for fitting, and the initial state are indicated.

Here, in the first "ordinary" representation, the retention was obtained by fitting to the initial state and then aim the curves toward the experimental data for lower degrees of saturation as compared to the initial state. Thus, no actual consideration to a relevant stress evolution was made, which will be discussed below. For higher degrees of saturation, as compared to the initial state, the retention curves appearance was not motivated.

In the second "new" representation, again with the initial state taken as a starting point, and assuming linear buildup of pressure with saturation together with using the free retention data, a confined retention curve was developed. For higher degrees of saturation as compared to the initial point, the extended Van Genuchten expression was fitted against the developed confined retention curve (where a relevant stress evolution was assumed, viz. the stress buildup during confined conditions), and for lower degrees of saturation as compared to the initial point the experimental data points were aimed at.

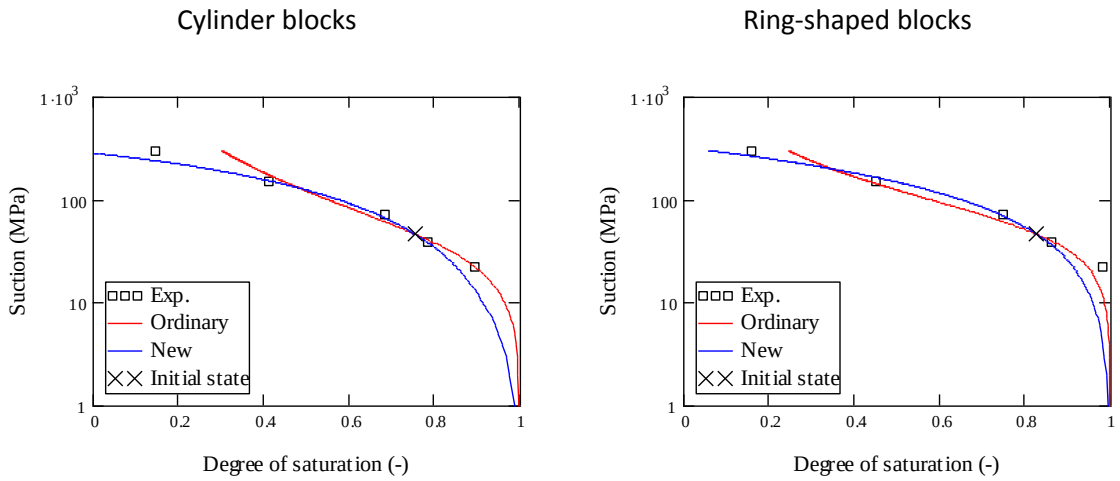

Figure 1 Ordinary and new retention curves together with experimental data and the initial state.

Results

The buffer saturation times (the time where $S_l \geq 0.99$ in the entire buffer), for all TH-simulations of a deposition hole performed in Åkesson et al. (2010), are shown in Figure 2. The horizontal lines represent the cases indicated to the right of the line where also the "mechanical assumption" (Homogenized state or Initial state) is indicated. Below the lower line (Init. Unfractured rock) the rock conductivity used are indicated. The hatched lines connect models with identical rock conductivities. Close to the lower line, the positions of the models where the buffer was altered are given (unfilled circles).

In the models the time until saturation in the buffer is most significantly dependent on the water transport properties of the surrounding rock. The distance to the hydraulic pressure boundary, presence of water bearing fractures, and the rock permeability are of great importance. In this work, when it comes to the distance to the hydraulic pressure boundary, the strategy was to study site data of the rock properties and developing a relevant representation. The rock permeability in turn, was varied in a wide range.

For the buffer material model alterations, the only significant effect on saturation time came from changing the block retention. When using 0.6 and 2 times the original buffer permeability, no significant change could be seen for the rock permeabilities that were used.

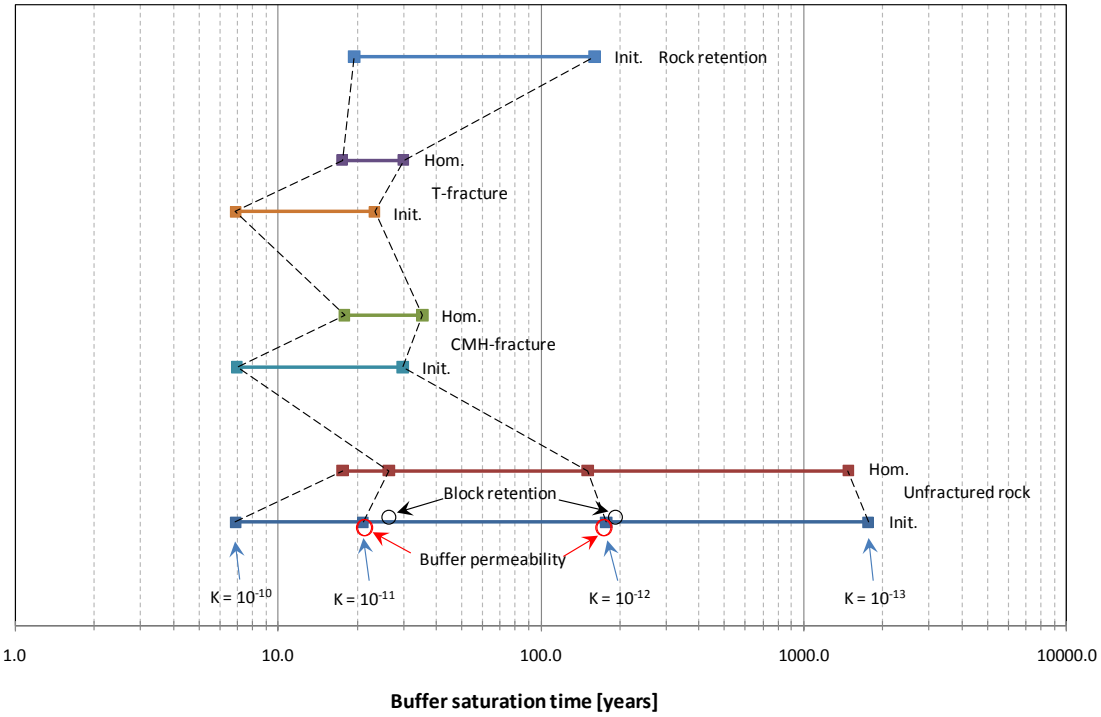

Figure 2 Compilation of the buffer saturation times (the time when Sl = 0.99 in the entire buffer) for all TH-simulations of a deposition hole. The text rightmost of the lines indicates the representation of the rock: Unfractured rock, CHM-fracture (fracture at canister mid-height), T-fracture (fracture at tunnel) and Rock retention (changed rock water retention curve). In the three first cases (from the bottom up) the buffer has been represented as in the initial state (Init.), where blocks and pellet slot are present, and as in a fully homogenized state (Hom.) as indicated to the right of the corresponding horizontal line. In the Rock retention representation case has only the Init. buffer representation been used. The results obtained using the same rock conductivity, indicated below the bottom line, are connected by hatched lines. The results from changing the Buffer permeability or Block retention are indicated by red or black circles, respectively.

Discussion/uncertainties

The saturation time for the buffer was seen to be affected by changes in the buffer retention. The retention curves used have been obtained by calibrating the expressions of Van Genuchten against experimental data, see Figure 1. Both errors in the experimental data and the capability of the utilized expression to be adapted to the real in-situ conditions are contributing factors to the uncertainty. The last of these factors, the adaptability, is discussed below.

When studying the subject of water retention of bentonite it is found that thermodynamics as well as experiments suggests the *in-situ retention* generally can be expressed in terms of *retention under free swelling conditions* and the *stress state*. Thus, it seems that in order to obtain a generally representative formulation, it should be based on the *retention for free swelling* and the current *stress state*.

Retention is known to be path dependent, which give rise to the characteristic hysteresis loop in retention for an absorption-desorption cycle as seen in Figure 3. Also characteristic are scan lines

obtained “within” the hysteresis loop, when changing from absorption to desorption and vice versa. Thus, a general representation of retention should include possibilities for hysteresis and scan lines. The Van Genuchten models used here cannot mimic these features.

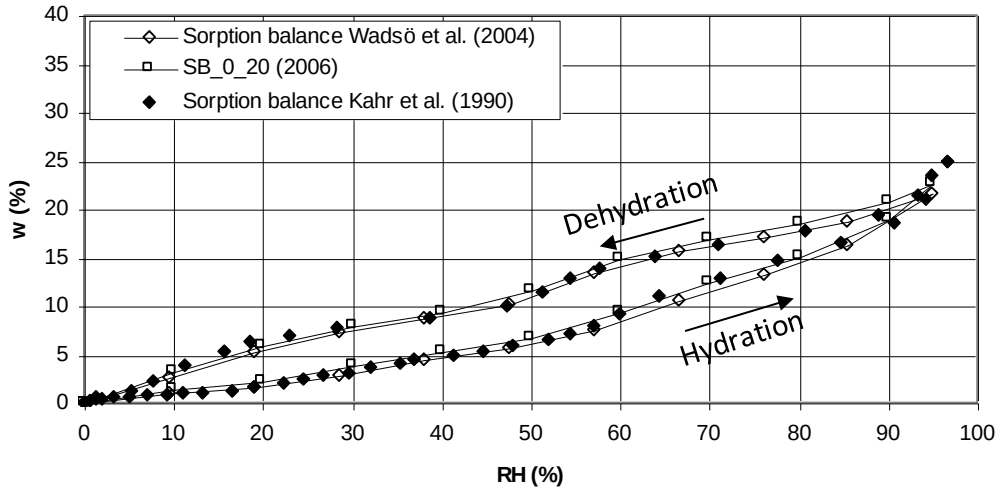

Figure 3 Retention curves determined for MX-80 bentonite.

When it comes to the stress state dependence of retention, a retention curve of Van Genuchten type does not contain this. Thus, if the real in-situ retention is believed to be dependent on the stress state, a stress evolution is implicitly assumed, when using Van Genuchten. If not thought of, the implicitly assumed stress evolution might be unrepresentative for the actual process the material is subjected to, which, in turn, would lead to improper retention characteristics.

When it comes to the *actual mechanism* of transportation of liquid through highly compressed bentonite clay it is not certain that the Darcy model correctly represents this. Taking a thermodynamical viewpoint when studying water flow in water saturated bentonite, the driving force is found to be the gradient of chemical potential rather than water pressure. If, however, the water pressure is considered to be a “representation” of the chemical potential, the outcome of the Darcy model corresponds well with to the thermodynamically motivated flow relation.

Task 4, Analysis of moisture redistribution in dry rock scenario (TH)

Result from this analysis, in form of thermal conductivities, served as input to the peak temperature calculations (Task 1). First an analytical investigation of the dehydration of the surrounding rock was performed. When performing the numerical analysis (using CODE_BRIGHT) of the moisture-redistribution, a hydraulic impermeable rock was assumed and cases with different hydraulic properties of the buffer were investigated.

For this task, important buffer material models are: the conductive heat flow,

$$\mathbf{i}_c = -\lambda \nabla T$$
$$\lambda = \lambda_{sat} S_l + \lambda_{dry}(1 - S_l)$$

, with parameters {λ_{sat}, λ_{dry}}, and the diffusion of vapor,

$$\mathbf{i}_g^w = -(n\rho_g(1-S_l)D_m^w)\nabla\omega_g^w$$

$$D_m^w = \tau 5.9\cdot 10^{-6}\frac{(273.15+T)^{2.3}}{p_g}$$

, with parameter {τ}.

When translating the obtained field of degree of saturation to thermal conductivity, the two relations shown in Figure 4, indicated by Alt 1. And Alt 2., respectively, were used.

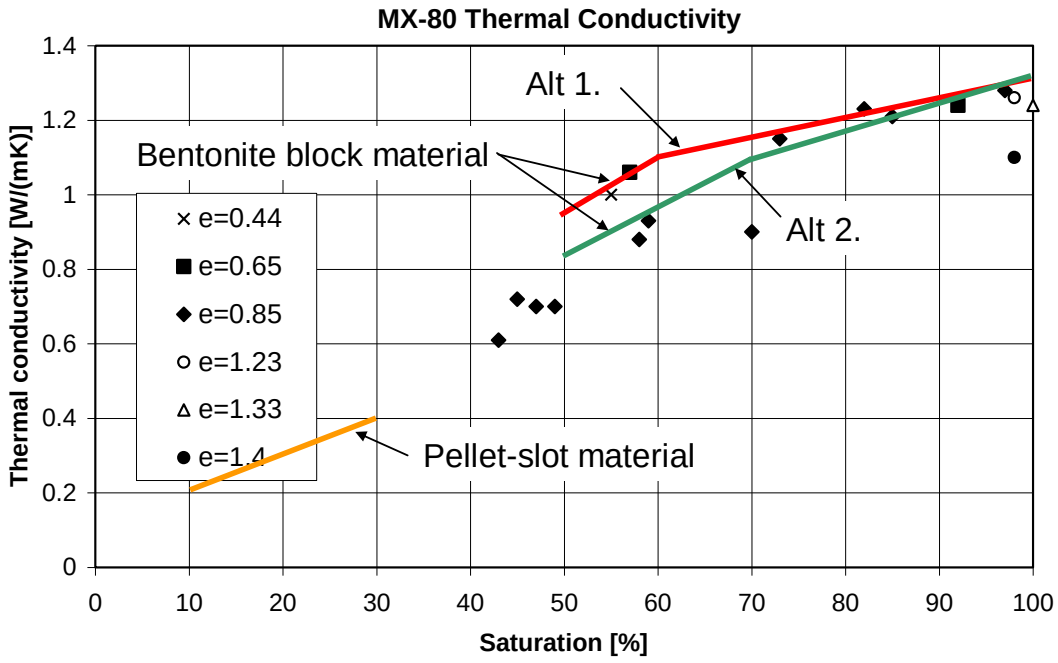

Figure 4 Thermal conductivity: experimental data and the functions used.

Results

As an example of a result obtained in this task, the evolution of the water saturation profile in the buffer is shown in Figure 5 below. In the next step, the saturation levels found, such as shown in Figure 5, were translated into spatially discretized thermal conductivities by use of two different relations between water saturation and thermal conductivity, so that an upper and a lower bound value were obtained.

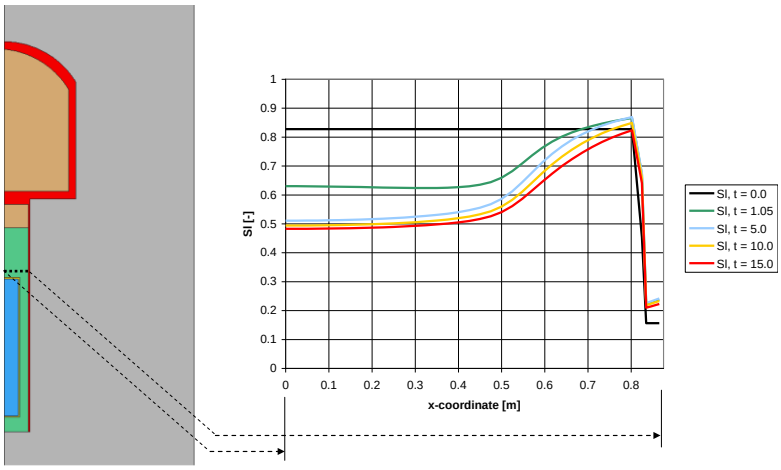

Figure 5 Water saturation profiles at the indicated horizontal scan line above the canister.

Discussion/uncertainties

The main outcome of this work has been to produce thermal conductivities, representative for the thermo-hydraulic problem, which may subsequently be applied in a pure thermal simulation. Therefore the translation process from the obtained field of water saturation into thermal conductivities is a relevant issue.

When translating the water saturation field into a discretized thermal conductivity field, a suitable mapping has to be used, both in terms of discretization and the relation between water saturation and thermal conductivity. By using two alternative relations between water saturation and thermal conductivity, see Figure 4, two sets of thermal conductivities were obtained, which may be used for bounding the thermal process within reasonable limits.

In a more general perspective, going outside of this particular task, dependencies of the thermal conductivity may be identified by studying the experimental data in Figure 6. The data suggest that, besides a dependence on degree of saturation, there is a dependence on density (void ratio). Thus, if the material undergoes large density changes and high accuracy is sought in the thermal solution, it could be of importance to incorporate a density dependency.

Also, when studying the experimental data in Figure 6, a linear dependency on degree of saturation (as used in this task) could be questioned if used for a wide range in degree of saturation. The graphs of three different expressions are shown together with experimental measurements in Figure 6. The red line (linear) is only valid at high degree of saturation, the black line (exponential) valid at somewhat lower degree of saturation, and finally the blue line (trigonometric) seem rather representative for all degrees of saturation.

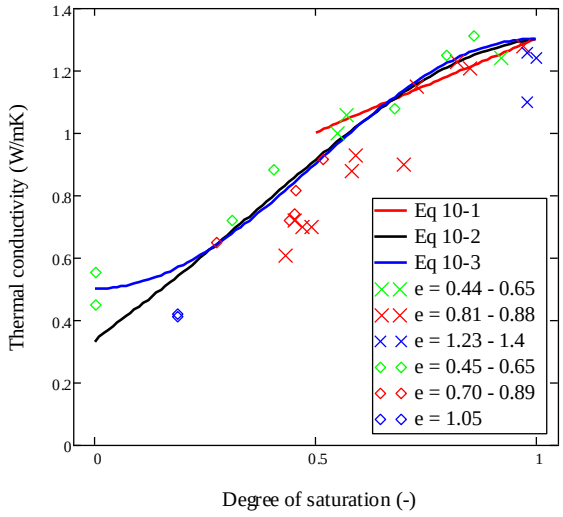

Figure 6 Thermal conductivity vs. degree of saturation: Experimental data and three alternative expressions.

Task 5, Buffer homogenization (THM)

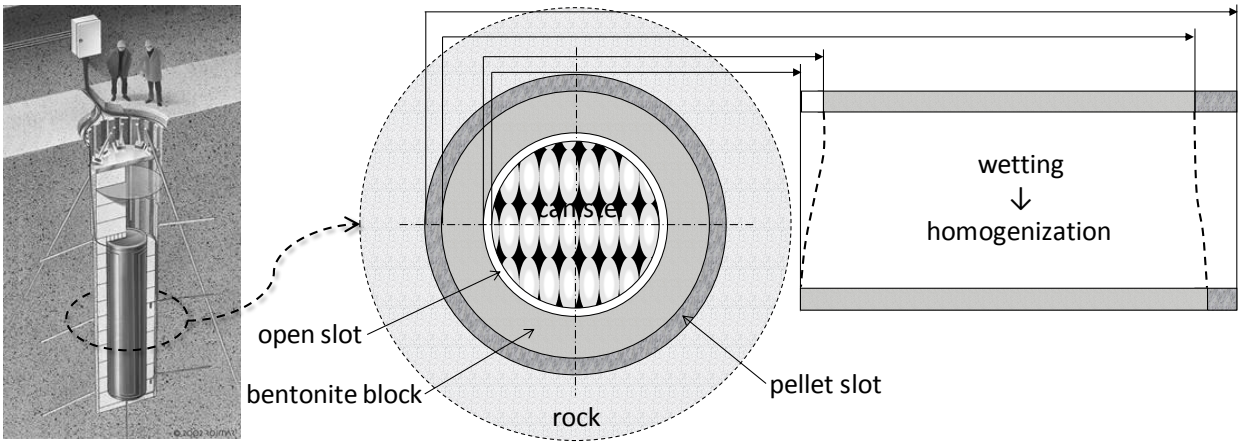

Figure 7 The Canister Retrieval Test geometry (left) and the model geometry where the homogenization process is studied (right)

The homogenization process of the buffer was here studied. Initially, at installation, the buffer consists of high density bentonite blocks, an outer slot between the blocks and the hole wall filled with bentonite pellets, and an empty inner slot between the canister and the blocks. When absorbing water, the clay swells and the buffer homogenize, see Figure 7. It has, however, been observed in full scale experiments that the system does not become totally homogenized at full water saturation. The remaining heterogeneity and the causes of this were here studied. The models were compared with data from a full scale field experiment, the Canister Retrieval Test (CRT), from which information of: initial state, the state during operation and the state after excavation was available. The models used in this task can be categorized as: analytical model, CODE_BRIGHT finite element (FE) models, and ABAQUS FE models.

The analytical model, with its basis in thermodynamics, was first used to investigate the influence of different wetting scenarios ("fast" or "slow") and different pressures in the block and pellet slot on the homogenization process in a buffer system consisting of block (*b*) and pellet filled slot (*p*). The analytical model,

$$s_{free}{}^{p}\left(\frac{\rho_w}{\rho_s}e^{p}\right)-\alpha\, s_{free}{}^{p}\left(\frac{\rho_w}{\rho_s}e^{b}\right)=0$$

$$s_{free}{}^{m}(w^m)=\exp\left(a^m-b^m\,w^m\right),\quad m=p,b$$

$$\alpha=p^{p}/\,p^{b}$$

, has parameters $\{a^b, b^b, a^p, b^p, \alpha\}$ where all parameters, except for α, are dependent on referential water content. The referential water content is defined as the water content from which absorption or desorption started.

The CODE_BRIGHT FE models were used for a detailed study of the homogenization process for a buffer ring at canister mid-height as shown in Figure 7. Models with different mechanical and hydraulic properties were first investigated. Thereafter, the effect from prescribing different pellet slot widths was studied. Finally, two extreme wetting scenarios were addressed. Comparisons between the analytical and the finite element models were also performed. For representing the mechanical buffer behavior an elastoplastic material model for soils, with its basis in Barcelona Basic Model (BBM), was used. BBM is formulated in a small strain framework, and therefore the total strain increment may be expressed as the sum of increments of strain. Three different increments of strain were used in this task: elastic, plastic, and hydraulic.

The elastic strain increment is defined by,

$$d\boldsymbol{\varepsilon}^{e}=-1/3\,d\varepsilon_{v}{}^{e}\boldsymbol{I}+d\boldsymbol{e}^{e}$$

$$d\varepsilon_{v}{}^{e}=\frac{dp'}{K},\ K=\max\left\{\frac{(1+e)\,p'}{\kappa_i(s)},K_{\min}\right\}$$

$$\kappa_i(s)=\kappa_{i0}\left[1+\alpha_i s\right]$$

$$d\boldsymbol{e}^{e}=\frac{d\boldsymbol{s}}{2G},\ G=\frac{3(1-2\nu)}{2(1+\nu)}K$$

, where $\{K_{\min}, \kappa_{i0}, \alpha_i, \nu\}$ are the parameters.

The plastic strain increment (active when $f = 0$) is defined by,

$$d\boldsymbol{\varepsilon}^p = d\Lambda \frac{\partial g}{\partial \boldsymbol{\sigma}}$$

$$f = q^2 - M^2(p'+p_s)(p_0 - p')$$

$$g = \alpha q^2 - M^2(p'+p_s)(p_0 - p')$$

$$M(p_0, p_s) = 0.5\left(\frac{p_0 + p_s}{2}\right)^{-0.23}$$

$$p_0(s, p_0^*) = p^c\left(\frac{p_0^*}{p^c}\right)^{\frac{\lambda_0 - \kappa_{i0}}{\lambda(s) - \kappa_{i0}}}$$

$$dp_0^* = \frac{1+e}{\lambda_0 - \kappa_{i0}} p_0^* d\varepsilon_v^p$$

, where $\{p_s, \alpha, p^c, \lambda_0\}$ are the parameters and the initial value $p_0^*(t = t_0)$ is to be specified.

The hydraulic strain increment is defined by,

$$d\boldsymbol{\varepsilon}^h = -1/3 d\varepsilon_v^h \boldsymbol{I}$$

$$d\varepsilon_v^h = \frac{\kappa_s(p', e)}{(1+e)(s + p_{atm})} ds$$

$$\kappa_s(p', e) = \kappa_{s0} f(p', e)$$

$$f(p', e) = \begin{cases} 1 & \text{if } p' < p_{ref} \\ 10^{-20} & \text{if } p' > p_{swell}(e) \\ 1 - \dfrac{\ln p' - \ln p_{ref}}{\ln(p_{swell}(e)) - \ln p_{ref}} & \text{otherwise} \end{cases}$$

$$p_{swell}(e) = 10^{\left[-4.741 + 4.117 \cdot 10^{-3} \frac{\rho_s}{1+e} - 3.94 \cdot 10^{-7}\left(\frac{\rho_s}{1+e}\right)^2\right]}$$

, where $\{p_{atm}, \kappa_{s0}, p_{ref}\}$ are the parameters. In the formulation above, two alternations of the original as given in CODE_BRIGHT has been used. The first is present in the expression of the plastic strain increment, where the critical state line parameter M has been made a function of p_0 and p_s (the latter being constant in this simulation). This modification was made in order to make the material model more in line with the experiments showing a pressure dependent shear stress at failure, see Figure 8.

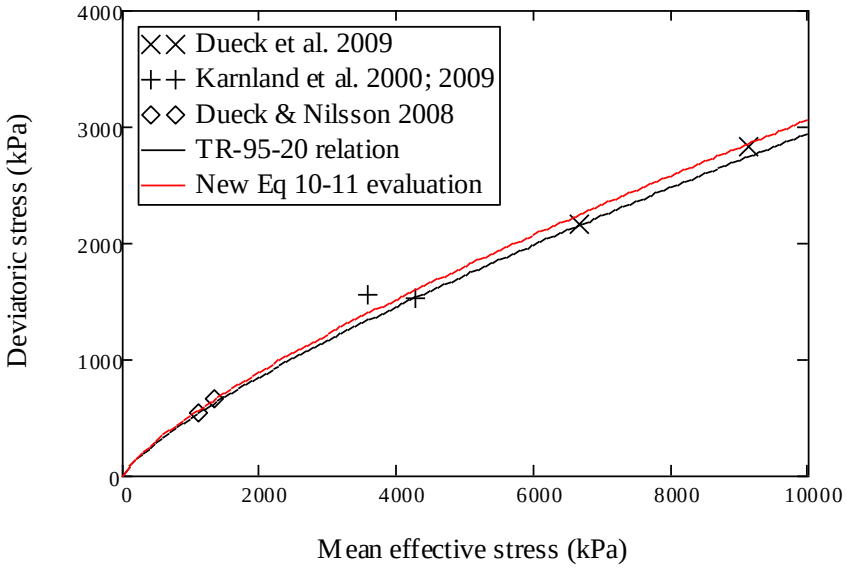

Figure 8 Deviatoric stress versus mean effective stress at points of failure.

The second alternation is present in the expression of the hydraulic strain increment, where swelling pressure dependence is incorporated in the "swelling-modulus" κ_s. This has been implemented in order to meet the characteristic appearance of the swelling pressure of bentonite showing strong density dependence, see Figure 9. To accomplish this, the swelling has been forced to stop by setting the swelling-modulus to zero when the pressure becomes higher than the adopted swelling pressure relation at the current density.

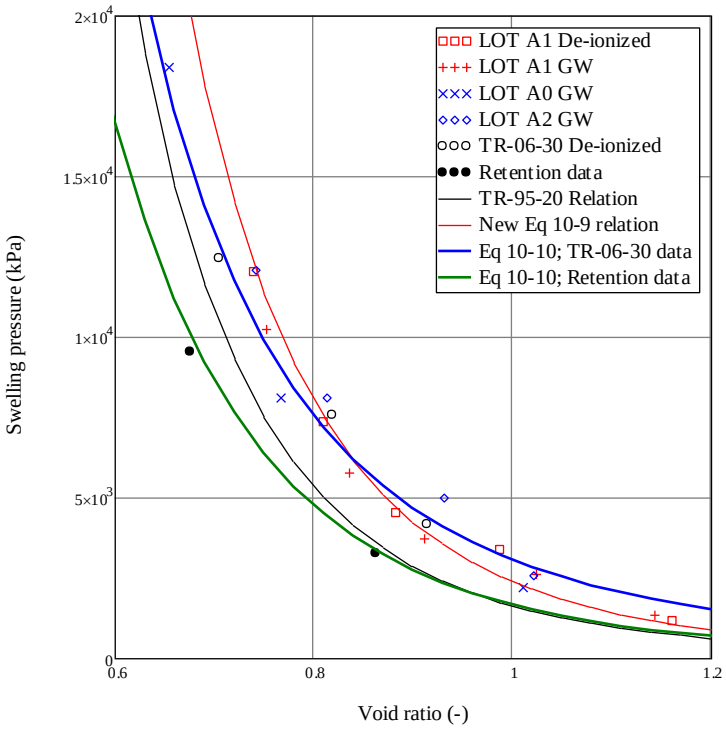

Figure 9 Swelling pressure measurements and different swelling pressure relations.

The results obtained from ABAQUS finite element models of the full scale CRT experiment were also shown. First, as a validation of the material models, a ring of the buffer at canister mid-height was represented by a 1D axisymetric model. Responses from this model were compared to CRT data and the CODE_BRIGHT solution. Then, using a 2D axisymetric model the entire experiment was simulated.

Results

The analytical model showed that the wetting process ("serial"=slow or "parallel"=fast in Figure 10), expressed by use of the wetting/drying retention curves of the clay, had a significant impact on the level of remaining heterogeneity of the buffer system. Also, the difference in total pressure in the block and pellet slot (indicated by the ratio α in Figure 10), was found to have a significant effect on the homogenization process. Figure 10 show a compilation of the findings of the analytical study.

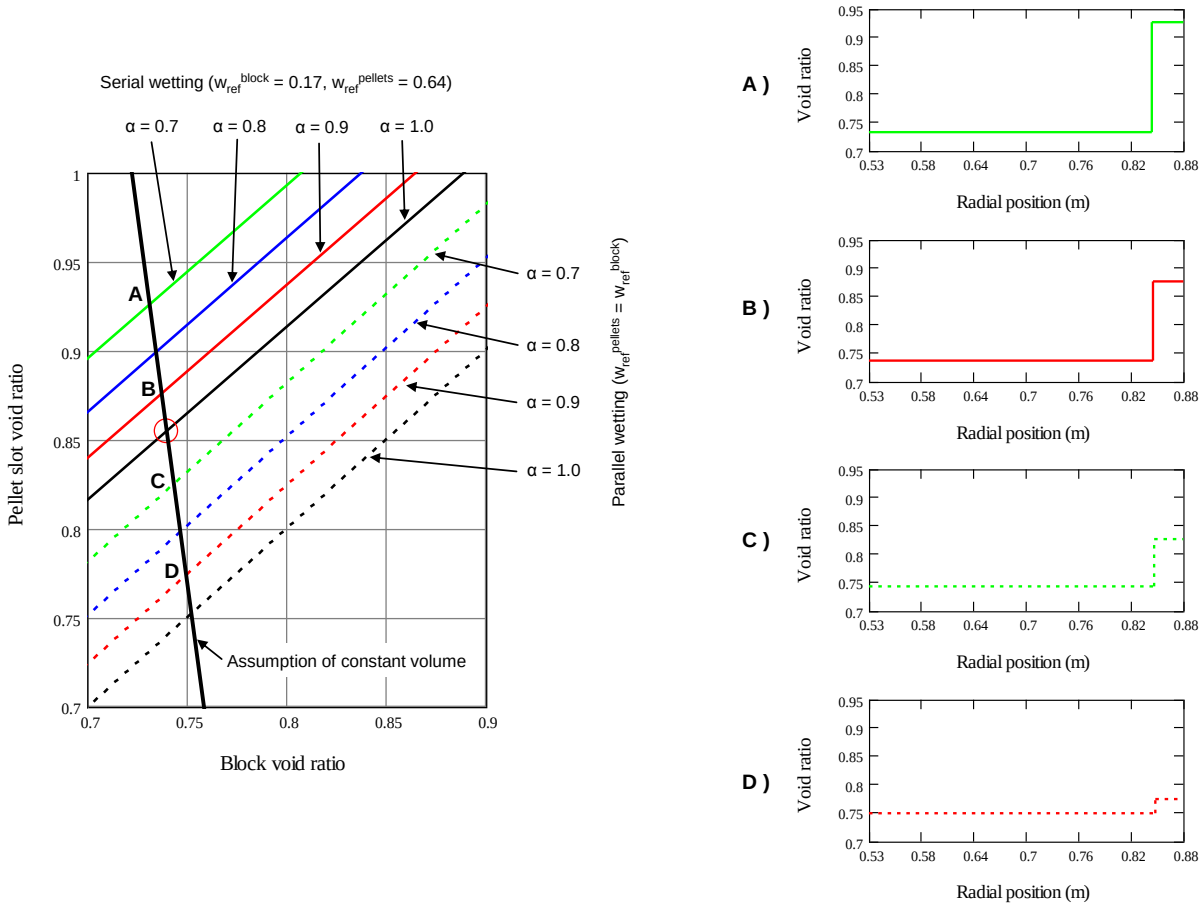

Figure 10 Compilation of the analytical model results for serial (solid lines) and parallel wetting (hatched lines) assuming different pressure ratios. The obtained average void ratio profiles are shown for four different choices in wetting process and pressure ratio along the constant volume assumption with the CRT state as a reference.

The CODE_BRIGHT finite element models of a ring of buffer at canister mid-height, where different pellet slot widths were considered, showed responses (Figure 11) that were in accordance with what was expected. The larger the slot, the higher the void ratios and lower the pressures at full water

saturation. The solutions of the finite element models and the corresponding analytical models agreed very well.

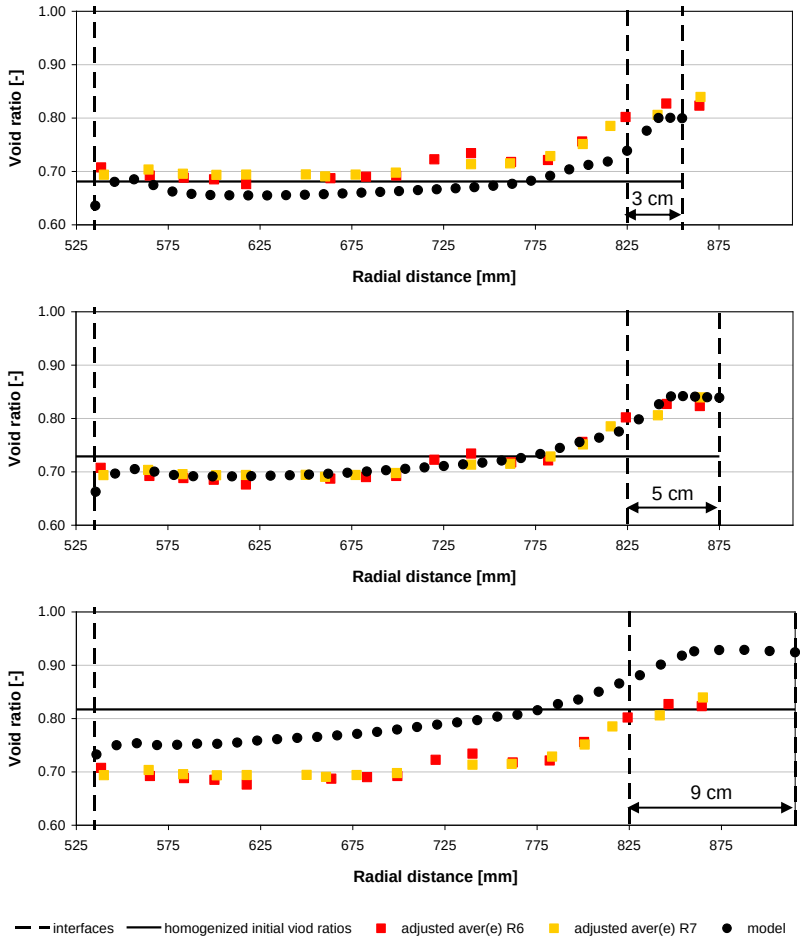

Figure 11 Void ratio profiles obtained for 3, 5 and 9 cm pellet slot. The markers squares and circles denote measurements and model calculations, respectively.

When performing the FE-simulation of the different wetting scenarios (serial="fast" or parallel="slow") it was not evident beforehand that the solutions (Figure 12) of the finite element model should agree well with the analytical solution. The analytical model indicated that different wetting scenarios were affecting the level of remaining heterogeneity, and in the analytical model this came from incorporation of path dependence in the retention. The finite element model did not, however, include this feature. Instead, the reason for obtaining the representative solutions with the finite element models came from the behavior of the modulus (κ_s) determining the swelling of the material when becoming more saturated.

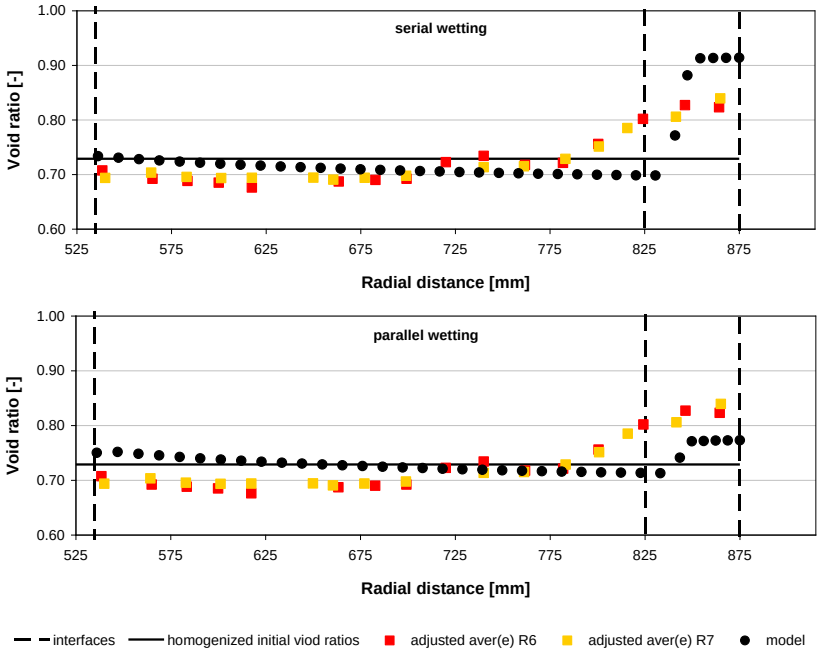

Figure 12 Void ratio profiles obtained for serial and parallel wetting.

The results from the ABAQUS finite element model of a ring of buffer at canister mid-height in CRT showed that the model were capable of capturing the processes in the experiment. Also, the solutions obtained from ABAQUS and CODE_BRIGHT were very similar. From studying the model it could be concluded that the homogenization process were completed at the end of the simulation and that heterogeneity still remained. When compared with experimental data, the evolution of the model responses agreed well except for the stresses that were generally about two times higher as compared with the experiment. Laboratory experiments have however shown that the used sensor installation give rise to artifacts (local low density volumes around the sensors) that explain this divergence. It should also be mentioned that all material parameters in the model were obtained from evaluating laboratory experiments and no “adaptation” was done in order to fit the model.

Finally, the entire CRT experiment was modeled using a 2D-axisymetric ABAQUS-model. The model was however continued in time, past when CRT was excavated, since the fully saturated state was sought for. At the end of the CRT experiment the buffer was far from being fully saturated at locations other then at canister mid-height. In the model, the last saturated point, at the top of the canister, was saturated after about 100 years. The solution gave a 3 cm upward swelling of the top-surface of the buffer (Figure 13), in the experiment constrained by a lid connected to the rock with wires to “simulate” the backfill compression. Generally, a rather heterogeneous density could be observed with higher density mainly below the canister and lower density close to the rock and especially in the “corner” between the buffer top surface and the rock, see Figure 13.

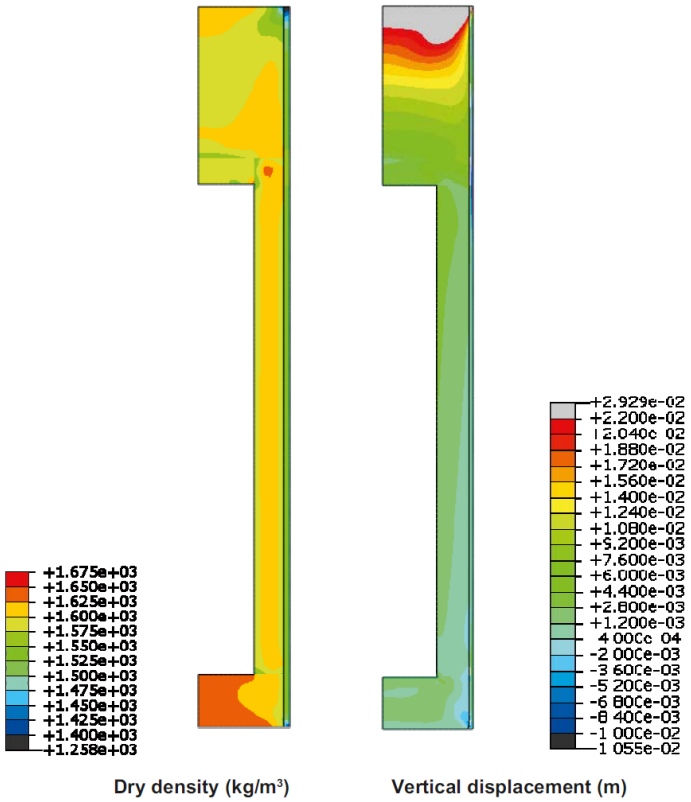

Figure 13 Final state of the buffer after full saturation and completed homogenization. The distribution of the dry density and the vertical swelling is shown.

The radial stresses were generally found to be considerably lower as compared to the axial stresses between the canister and the rock. At the same "corner" where low density could be observed, low pressure was also found.

Discussion/uncertainties

Analytical model

The analytical model heavily relies on "free" retention curves (i.e. retention curves obtained under free unconfined swelling conditions). Available representative retention curves are therefore crucial for this model. To be able to represent material undergoing different wetting scenarios it's necessary to have both accurate wetting and drying curves.

Improvements of the model could be done by considering the transition states (belonging to the so called scan lines), when going from wetting to drying and vice versa. The analytical model could also be generalized to consider not only isotropic mechanical states (i.e. only considering pressure and volume increments), but also embrace multiaxial states, where entire stress and strain tensors enters the formulation.

CODE_BRIGHT models

When it comes to the CODE_BRIGHT models the most significant uncertainties probably comes from the mechanical material model (here the modified version of BBM) and the model representing the retention properties (here given as a relation between water saturation and suction, by the Van Genuchten model). Below some issues related to the mechanical material model are discussed.

What is believed to be characteristic properties of bentonite clay, found from analyzing experimental data, are sometimes hard to mimic with the used mechanical constitutive law. BBM also has a rather extensive number of parameter values to specify and due to lack of experimental data (or rather, data of specific dedicated experiments needed) the uncertainties in the adopted parameter values might be significant. Parameters evaluated from available data, may also exhibit dependencies on variables that are not supported in the model. In these cases a suitable value of the parameter has to be estimated with the model behavior in mind for the specific process considered. Thus, the model will suffer from a limited range of validity and become rather process dependent.

As discussed above in the model description, some of the characteristic features of compacted bentonite, such as the swelling pressure curve shown in Figure 9 and failure envelope shown in Figure 8, have been used as a basis when developing BBM towards better capabilities of representing bentonite. This might be taken further by for instance incorporating direct couplings between retention and the mechanical material model, and deriving expressions for other parameters from fundamental relations.

The deficient connection between the BBM-framework and the behavior of bentonite might stem from that BBM has a rather general phenomenological basis, valid for a broad range of geomaterials, but that bentonite, in a sense, is not a typical geomaterial. One reason for this could be that the underlying mechanisms, governing the material characteristics, might work on a rather different scale (the montmorillonite mineral layers have interlayer distances on the nm-scale) as compared to typical geomaterials (sand, silt etc.).

One finding that could support this view, is that when adopting a thermodynamical/chemical viewpoint, and considering the buffer material a mixture of clay mineral, salt, water etc. estimates of the material characteristics are obtained that correspond very well to experimental data. In the scientific field of colloid chemistry this view is common and widely accepted for montmorillonite. This is for instance the case in the well known DLVO theory, applicable for montmorillonite. Moreover, this “small-scale-view” is not isolated from mechanics. When considering overlapping double layers, present in interlayers between neighboring montmorillonite mineral layers, the concept of swelling pressure naturally arises.

Thus, phenomenological models developed with typical geomaterials in mind, might have shortcomings when simulating bentonite clay. A well designed and specifically dedicated bentonite material model might be beneficial for obtaining more general simulations, where parameter values do not need to be prescribed differently for different processes. Also, the results obtained from the thermodynamical/chemical viewpoint mentioned above, strongly suggests that a suitable path might be if a material model was developed with thermodynamical/chemical considerations in mind.

One issue that is not very influential for the geometry used here, but that might be significant for more unconstrained deformations, is that CODE_BRIGHT uses a small strain formulation. The small strain assumption is based on that second order terms in the displacement gradient are negligible as compared to first order terms.

ABAQUS models

Also in these models, as well as for the CODE_BRIGHT models, the main uncertainty stem from the material models. The material models are complicated and the values of the belonging parameters

can therefore be hard to determine accurately. Although the material models have been verified in the 1D case, the consideration when moving to 2D give more degrees of freedom and generally complicate the modeling. In the 2D model a friction model, used to mimic the interaction between the bentonite block and rock-wall or canister-surface, also increases the complexity of the simulated system.

Task 6, Homogenization after loss of bentonite mass (HM)

The homogenization process (due to the expansion of bentonite when wettened), in cases where buffer mass is lost, was here addressed. Loss of the buffer might come from: improper installation, erosion (caused by colloidal formation or water inflow), and piping.

Homogenization was investigated by using three different geometry categories of ABAQUS FE-models corresponding to different cases of buffer mass loss:

1. a large part of the buffer is missing (long time colloid erosion or mistakes at installation),
2. local parts of the buffer is missing (water inflow erosion), and
3. an open channel is formed in the buffer (formed by piping and erosion).

Results

The friction between the buffer and rock/canister is significantly affecting the homogenization process. Due to the large swelling, large magnitudes of deformation/strain occur. The density variation at the final stage is significant.

Uncertainties

It is of importance to be able to represent the rock/canister friction correctly in order to obtain relevant simulations. Also, the mechanical buffer material model has to be general in the sense that it is valid for a wide density range. The model, as well as the numerical scheme, should be able to handle large deformations/strains.

Task 8, Buffer upward swelling (HM)

The effect of homogenization between buffer and backfill on the buffer density distribution was here studied. ABAQUS FE-models with different height of the stack of backfill blocks above the deposition hole, as well as different initial buffer density, were used. To simplify the calculations, here the fully coupled and concurrent homogenization process during water saturation of the buffer and backfill (as considered in Task 5) was not considered. The utilized technique may be thought of as if the homogenization process was considered a two-step sequence, where first the buffer was completely homogenized under confined conditions, and then let to interact with the surroundings (e.g. the backfill material), here held at the initial level of water saturation. In this way, the numerical simulation started from when the buffer was totally saturated, totally homogenized, and pressurized with the confining swelling pressure, expected at the prescribed density.

Results

The models showed a significant vertical upward deformation. Variation in the buffer density gave less upward swelling and lower values of swelling pressure. Different heights of the stack of backfill block did not give any significant changes in responses.

Uncertainties

The coupling between buffer upward swelling and buffer density implies that the correctness of the mechanical material model is of importance for obtaining relevant simulations.

If there is a significant intrinsic path dependency in this problem, the used solution scheme might not be able to pick this up. Path dependency is known to be present in the buffer retention behavior, the buffer mechanical behavior, and in the pressure dependent friction process between buffer and rock/canister in the present problem.

Task 9, Canister sinking (HM)

Canister settlement caused by the influence from canister weight and upwards swelling of the buffer/backfill interface was here investigated. Two types of ABAQUS FE-models were utilized:

1. when only the effect from canister weight were considered and
2. when effects from both canister weight and upwards swelling of the buffer/backfill interface were considered.

The solutions of the two extreme cases are used as limits.

Results

The study showed that the displacement of the canister, from consolidation and creep, during 100 000 years is very small. The model show very low sensitivity to reduced density or reduced friction angle (shear strength).

Uncertainties

Since the model simulates such long time span and the creep model can only be validated in laboratory experiments during shorter times, the validity of the creep model over time cannot be proven.

Task 10, Rock shear trough a deposition hole (HM)

The effect from rock shear through a deposition hole was here investigated. The buffer can be thought of having a damping effect on the rock motion and only transferring this partially toward the canister. ABAQUS FE-models with varying shear rates and shear directions were equipped with a rate dependent (viscous) mechanical material model representing the buffer.

The calculations have been performed in a separate project and have also been reported separately, see Hernelind (2010).

Task 11, Piping and erosion (HM)

An estimate of the loss of mass of the buffer due to piping and erosion in was evaluated in this task. When high point inflow of water occur at the wall of a deposition hole towards the buffer, “pipes” might be formed in the buffer under certain conditions, where water may flow more freely. At the walls of the formed pipes, buffer material might be eroded and transported by the water flow. The estimations of the loss of mass were performed by use of an empirically derived model, developed

by fitting an expression against experimental data. The model input was accumulated mass of eroding water and two parameter values, and the output accumulated mass of eroded bentonite.

Results

Using the model together with rather conservative assumptions regarding the accumulated mass of eroding water (all the available volume in a tunnel with 50 deposition holes are to be filled from the eroding outflow of one deposition hole), an estimated range of eroding mass of buffer is obtained.

Uncertainties

The model is not based on considerations of the underlying mechanisms, but merely fitting a chosen expression's parameters so that it resembles the appearance of experimental data. On the other hand, if the experimental setup is close to (or contains) the case that is studied by the model, the probability for the solutions to be reliable is high.

Task 18, Bottom plate 1 – Lifting of package (HM)

The objective of this task was to analyse the potential lifting of the buffer and canister package during the period from the termination of the drainage to the installation of the backfill, if a water-bearing fracture intersects the deposition hole beneath the bottom plate. An analytical model was derived for evaluating if the package would lift, and if so, how long time it would take before the package would lift for different fracture inflows.

The model indicates that the time to reach lifting conditions is approximately one week. With that said, this task will not be discussed further.

Task 19, Bottom plate 2 – Buffer swelling after concrete disintegration (HM)

This task addressed the buffer swelling into the volume created after disintegration of the concrete in the bottom plate. Essentially, the same model as used in Task 8 was utilized, with the difference of the allowed subsequent downward swelling, of up to 6 cm, of the buffer at the hole bottom.

This particular task will not be discussed further since the uncertainties of this type of model have been addressed before (in describing task 8).

References

Hernelind J. (2010). Modelling and analysis of canister and buffer for earthquake induced rock shear and glacial load. SKB TR-10-34. Svensk Kärnbränslehantering AB.

Hökmark H., Sundberg J., Kristensson O., Lönnquist M., and Hellström G. (2009). Strategy for thermal dimensioning of the final repository for spent nuclear fuel. SKB R-09-04, Svensk Kärnbränslehantering AB.

Åkesson M., Börgesson L., and Kristensson O. (2010a). SR-Site Data report, THM modelling of buffer, backfill and other system components. SKB TR-10-44, Svensk Kärnbränslehantering AB.

Åkesson M., Kristensson O., Börgesson L., Dueck A., and Hernelind J. (2010b). THM modelling of buffer, backfill and other system components. Critical processes and scenarios. SKB TR-10-11, Svensk Kärnbränslehantering AB.